A new climate chamber for air-source and ground-source heat pump testing based on the Hardware-in-the Loop approach: Design and cross validation

Matteo Dongellini, Vincenzo Ballerini, Gian Luca Morini , Claudia Naldi, Beatrice Pulvirenti, Eugenia Rossi di Schio, Paolo Valdiserri

A new climate chamber for air-source and ground-source heat pump testing based on the Hardware-in-the Loop approach: design and cross validation

In: Journal of Building Engineering, Volume 64, 2023, 105661

The final published version is available online at:

https://doi.org/10.1016/j.jobe.2022.105661

A new climate chamber for air-source and ground-source heat pump testing based on the Hardware-in-the Loop approach: design and cross validation

M. Dongellini, V. Ballerini, G.L. Morini , C. Naldi, B. Pulvirenti, E. Rossi di Schio *, P. Valdiserri

Department of Industrial Engineering, Alma Mater Studiorum - University of Bologna, Viale del Risorgimento 2, 40136 Bologna, Italy;
matteo.dongellini@unibo.it; vincenzo.ballerini2@unibo.it; claudia.naldi2@unibo.it; beatrice.pulvirenti@unibo.it; gianluca.morini3@unibo.it; eugenia.rossidischio@unibo.it; paolo.valdiserri@unibo.it

*Correspondence: eugenia.rossidischio@unibo.it; Tel.: +39-051-209-3294

Abstract: The present paper describes a new test bench, designed for experimental tests on small- and medium-sized air-source and ground-source heat pumps, built at the University of Bologna (Italy). The test rig is based on the “Hardware-in-the-Loop” approach and is mainly composed of a test room (i.e. the climate chamber), in which the tested heat pump is placed, a borehole heat exchanger field for tests on ground-source units, the hydraulic loop and the building emulator. The test rig allows to test commercial and prototypal heat pumps under dynamic operating conditions, in order to reproduce the real behavior of a heat-pump based heating system and assess the heat pump effective energy performance. According to the Hardware-in-the-Loop approach, the hydraulic circuit of the facility is designed to reproduce exactly the time-dependent variations of the weather data during a series of representative days in a chosen site and the building thermal load given to the heat pump, calculated by a dynamic simulation software (i.e., the building emulator). In this paper, main components of the experimental facility are presented and the outcomes of a series of numerical simulations carried out with different software, such as Trnsys, Matlab-Simulink and STAR-CCM+, to define the system operative range and the effective behavior of the test bench under dynamic conditions are reported. Numerical models have been validated with experimental data, obtained from a trial test carried out on an air-source heat pump according to current technical standards. Comparison between numerical data and experimental results point out an excellent agreement and, for this reason, numerical models can be used to assess the optimal position of the tested heat pump within the chamber or to define the test bench operating

conditions. The cross-validation methodology between experimental data and numerical results from different software, applied in this paper to a test bench for heat pumps, can be employed for the sizing of other test facilities.

Keywords: Climate chamber; Hardware-in-the-Loop, heat pumps, dynamic tests, control strategy, CFD

1. Introduction

In Europe, the recent REPowerEU Plan [1] aims to fast forward the green transition, by increasing, among the others, from 40% to 45% the headline 2030 target for renewables, fixed by the European Directive 2018/2021 at 32% [2].

In this frame, heat pumps can meet the energy demand of buildings, by maximizing the exploitation of renewable energy linked to air, ground or water [3, 4]. In Europe, the most widespread typology is represented by air-source heat pumps (ASHPs), as revealed by recent market data [5]. ASHPs, compared to ground-coupled heat pumps (GCHPs), are cheaper and easier to install, although they have some disadvantages. First of all, the performance of an ASHP is lower when the outside temperature decreases, while the energy demand of the building increases. For this reason, an alternative strategy to design a heating system based on an ASHP could be coupling the heat pump with a back-up system. Dongellini et al. [6] focused on the importance of the correct sizing of the heat pump in presence of both electrical and fossil fuel-based back-up systems to obtain the best seasonal efficiency. Bagarella et al. [7] demonstrated how the heat pump sizing influences the annual performance of hybrid heating systems, in which a gas boiler is used as back-up heater. In addition, they showed that the thermal storage sizing and the transient phenomena linked to the heat pump start-up can influence the annual performance of the system.

The frosting phenomenon, particularly in cold and damp climates, is an additional problem of ASHPs [8-10]. Defrosting cycles are usually activated during the winter when the outdoor temperature drops below 6°C and the air relative humidity is higher than 50%. It is well established how defrosting techniques reduce the energy performance of the heating system, as described by Rossi di Schio et al. [9], as well as the thermal comfort in heated environments, as underlined by Vocale et al. [11].

Conversely, GCHPs are more efficient than ASHPs, because they are able to use an external thermal source as the ground thermally more stable than air along the year [12]. Nevertheless, GCHPs are more expensive than ASHPs, since they need to couple the heat pump with a dedicated borehole heat exchanger (BHE) field. Moreover, the drift of soil temperature can significantly reduce the performance of GCHP systems. As underlined by You et al. [13], in fact, the GCHP energy performance significantly decreases in presence of buildings with unbalanced thermal loads between winter and summer. In case of a predominance of the building heating loads with respect to cooling loads and with a non-optimal sizing of the BHE field, the ground temperature can decrease year by year. This fact introduces a penalization on the energy performance of the GCHP and, in some cases, even to a system failure [13]. Moreover, in a BHE field a crucial role is played by the circuit arrangement [14]. Performance differences between ASHPs and GCHPs have been recently shown by Safa et al. [15] in a comprehensive study, comparing experimental and numerical results, and by Self et al. [16]. In addition, during last years, alternative heat pump solutions have been developed and several works can be found in the open literature. Urban sewage source heat pumps (USSHPs), investigated by Zhao et al [17], solar-assisted heat pumps and trans-critical CO_2 heat pumps, studied by Ran et al. [18] and Quirosa et al. [19], respectively, have been introduced to increase the exploitation of renewable energy sources and reduce carbon emissions in the building sector.

A possible solution to the drawbacks of both ASHPs and GCHPs are hybrid systems. These systems can be divided into two categories: (i) hybrid systems composed by multiple generators or (ii) hybrid systems based on a single generator that can exploit different thermal sources (e.g. air and ground with the same device). The latter case can be obtained adopting a dual-source heat pump (DSHP) able to exchange heat with two different external thermal reservoirs. The definition of “dual-source heat pump” has been also used to indicate hybrid systems based on multiple generators, as described by Lazzarin [20]. The author investigated on the energy performance of heating systems based on two heat generators: an ASHP coupled to solar thermal collectors and a GCHP coupled to the same solar collectors field. On the contrary, data about the performance of a DSHP able to exploit energy from different external heat sources are still limited in the literature. Grossi et al. [21] analyzed the seasonal and yearly energy performance of a DSHP able to exploit thermal energy from both the ambient air and the ground, coupled to a one-storey single-family house located in the North of Italy. The authors conducted a

series of experimental tests to obtain the characteristic curves of an innovative prototype of DSHP and, according to the experimental results, they designed a Trnsys [22] model for the evaluation of the DSHP energy performance by varying the size of the borehole field and the heat pump control strategy. The performance indicators are compared with those obtained using the DSHP as a full air-source heat pump (air-source mode) or as a full ground-coupled heat pump (ground-source mode) with the aim to explore in which operative conditions a DSHP can be competitive with the conventional monovalent systems based on heat pumps.

In the present study, a new test facility has been designed and constructed to evaluate experimentally the energy performance of different typologies of heat pump under dynamic operating conditions. Since in-situ monitoring of heat pump-based systems in occupied residential and commercial buildings is expensive and authorizations from the occupants are strictly needed, the test bench described in this paper is a convenient facility to test the effective behavior of this kind of systems. In fact, as recently underlined by Valdiserri et al. [23], who designed a climate chamber for tests on tracked and wheeled tractors, the development of laboratory facilities for experimental tests is fundamental for both industrial and academic bodies to obtain reliable data.

The test rig has been conceived to control the tested heat pump employing a “Hardware-in-the-loop” (HiL) approach. The HiL methodology is a sophisticated and accurate procedure to study the performance of heat pumps coupled to buildings. Haves et al. [24], Lahrech et al. [25] and Anderson et al. [26] have shown that experimental tests on complex heating systems are possible through the use of climate rooms which reproduce on-time the external conditions that the systems would face in the real case. De La Cruz et al. [27] published the implementation of a HiL real-time simulation test bench for heat pumps, demonstrating that this approach is suitable to test innovative control logics for heat pumps and reduce cost and time required for the heat pump development-to-market process. Conti et al. [28] demonstrated the relevance of a dynamic analysis of the building-HVAC system and the potential of the HiL approach in assessing heat pump performance at partial load. Frison et al. [29] tested a model-predictive control algorithm in a HiL environment. Following the approach of the Hardware-in-the-Loop concept, Mehrfeld et al. [30] performed a round-robin test to verify the experimental process and its results for three energy conversion systems: an ASHP, a GCHP and a micro combined heat and power system.

. .

In the present paper, the layout of a new test bench, based on the HiL approach, and the main features of its components are described. The test rig is suitable to test small- and medium-sized air-source and ground-source heat pumps, as well as dual-source units, by assessing their performance experimentally or by developing innovative control logics. The heat pump under test is placed within a climate chamber (CC), coupled to the hydronic circuit of the test rig. A field made of four vertical borehole heat exchangers (BHEs) is connected to the circuit to test GCHPs in real operating conditions. Finally, a dynamic simulation software, namely the building emulator (BE), is used to calculate the building thermal load and set both the values of air temperature and relative humidity that have to be reproduced in the CC, according to climatic data given by the BE. The role of numerical simulations for the design of the experimental test rig has been crucial. In fact, the behavior of both the climate chamber and the hydronic loop under transient conditions has been evaluated numerically during the design phase by means of two dynamic simulation software. More in detail, Trnsys [22] and Matlab-Simulink [31] have been selected as simulation tools. Each component of the test rig has been modelled with both software, allowing a more precise prediction of the sytem behavior for design and off-design conditions and a cross-comparison of numerical results. The open-source Simulink toolboxes Carnot [32] ALMABuild [33] have been used to model the whole test bench.
Furthermore, in this paper results from an experimental test carried out to determine the performance of a commercial ASHP according to current technical standards are reported as reference. Experimental data have been used to validate a CFD numerical model of the climate chamber, developed with STAR-CCM+. The optimal position of the tested heat pump and the chamber operating conditions have been defined according to numerical outcomes from the model. The cross-validation methodology described in this paper, based on the use of different software, can be employed during the design phase of other test facilities dedicated to heat pump testing.

2. Experimental test rig

As mentioned in the previous Section, the experimental test rig is composed of a climate chamber, a building emulator and a hydronic loop (HL), coupled to a borehole heat exchanger field.

2.1 Climate chamber

The climate chamber is a room having an internal net volume of 78 m^3, dimensions 6.40 m (length) × 4.35 m (width) × 2.80 m (height), for a net floor area of 27.8 m^2. A simplified layout of the CC is represented in Figure 1. The lateral walls and the ceiling are very well insulated, with a polystyrene layer of 30 cm, in order to reduce the heat transfer between the room and adjacent zones. In Table 1, thermo-physical properties of the climate chamber envelope components are reported. Each wall is identified with an acronym, as shown in Figure 1, from A to D. Only wall D is exposed to external air; other three vertical walls and the ceiling are adjacent to other internal zones of the laboratory, while the floor lies on the ground. Data reported in Table 1 highlight how the U-value of external walls and ceiling is about 0.1 W/m^2K, while the floor has a transmittance of about 2.31 W/m^2K. Wall A also presents a door of 2.58 m^2, thickness equal to 0.07 m and U-value of 0.565 W/m^2K.

The hydraulic scheme of the test bench is shown in Figure 2. Inside the CC, three air-heaters (Figure 3a), whose technical specifications are reported in Table 2, are installed (components 1, 2, 3 in Figure 2). Air-heaters have different nominal heating capacity and each of them is equipped with an inverter-driven fan. The air flow rate managed by air heaters ranges between 150 and 12100 m^3/h. A series of immersed electrode humidifiers are also planned to be installed to maintain the indoor relative humidity at the desired set-point value.

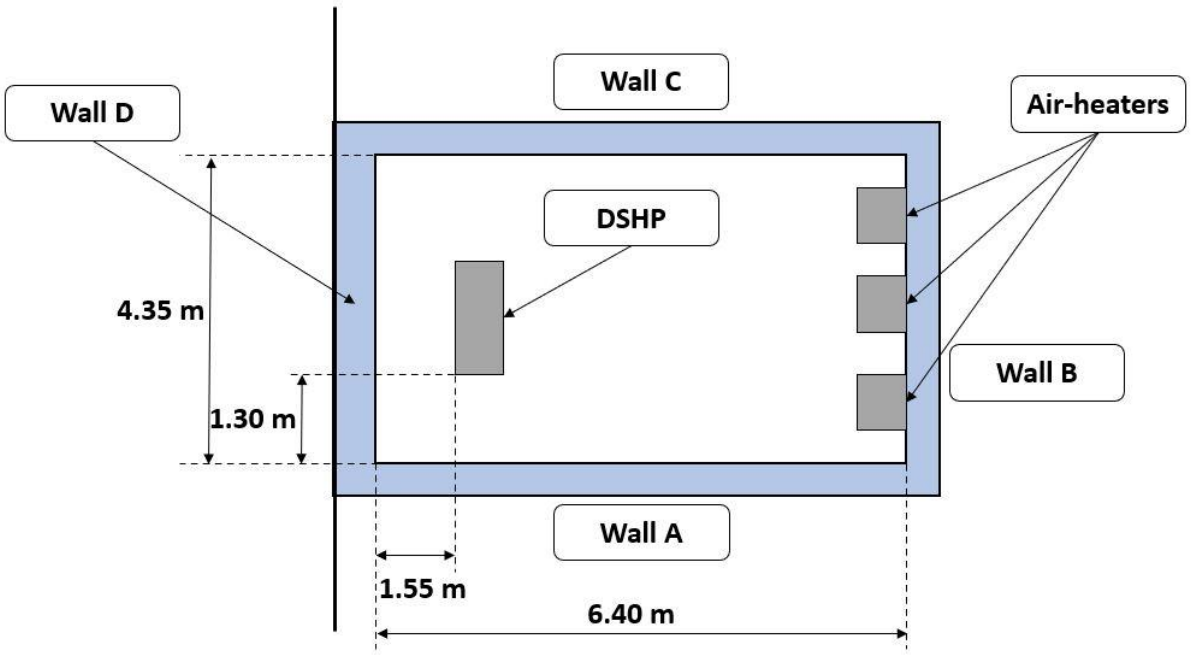

Figure 1. Simplified layout of the climate chamber, with dimensions, wall positions and displacement of devices.

Table 1. Thickness and thermo-physical properties of the climate chamber envelope components (layer structure from inside to outside).

Wall/Surface	Envelope Component	Thickness (m)	U- value (W/m^2K)	Thermal conductivity (W/mK)	Density (kg/m^3)	Thermal capacity (J/kgK)
Wall A		0.326	0.104			
	Plasterboard 1	0.013		0.35	1150	1000
	Plasterboard 2	0.013		0.25	740	840
	Insulant	0.300		0.032	32	1700
Wall B		0.546	0.095			
	Plasterboard 1	0.013		0.35	1150	1000
	Plasterboard 2	0.013		0.25	740	840
	Insulant	0.300		0.032	32	1700
	Plaster	0.020		0.9	1800	910
	Thermal blocks	0.200		0.24	780	840
Wall C		0.596	0.092			
	Plasterboard 1	0.013		0.35	1150	1000
	Plasterboard 2	0.013		0.25	740	840
	Insulant	0.300		0.032	32	1700
	Plaster	0.020		0.9	1800	910
	Thermal blocks	0.250		0.21	600	1000
Wall D		0.476	0.100			
	Plasterboard 1	0.013		0.35	1150	1000
	Plasterboard 2	0.013		0.25	740	840
	Insulant	0.300		0.032	32	1700
	Hollow bricks	0.120		0.35	800	1000
	Plaster	0.030		0.9	1800	910
Ceiling		0.526	0.100			
	Plasterboard 1	0.013		0.35	1150	1000
	Plasterboard 2	0.013		0.25	740	840
	Insulant	0.300		0.032	32	1700
	Concrete	0.180		0.59	1600	1000
	Mortar	0.020		0.73	1850	1000
Floor		0.123	2.306			
	Mat	0.005		0.17	1200	1400
	Insulant	0.018		0.38	1200	840
	Dry screed	0.020		0.39	1850	1000
	Concrete	0.080		0.59	1600	1000

2.2 Hydraulic scheme of the test rig

Since the main application of the climate chamber is to study the behavior of heat pumps under dynamic operating conditions, it is mandatory to control the ambient conditions within the CC when an ASHP is tested, using both air heaters and humidifiers. In fact, when an ASHP is operated in heating mode, the CC air temperature is reduced by the evaporation of the refrigerant fluid. To maintain the CC temperature at the desired value, the heat supplied by the heat pump condenser can be used. The hot water produced by the heat pump is used to feed the air heaters placed in the chamber through the hydronic loop shown in Figure 2. In this way, the CC air temperature can be controlled balancing the heat absorbed by the heat pump with that introduced in the chamber by internal air heaters. Internal air temperature can be modified by varying the air heaters fan speed, increasing or decreasing the heat supplied.

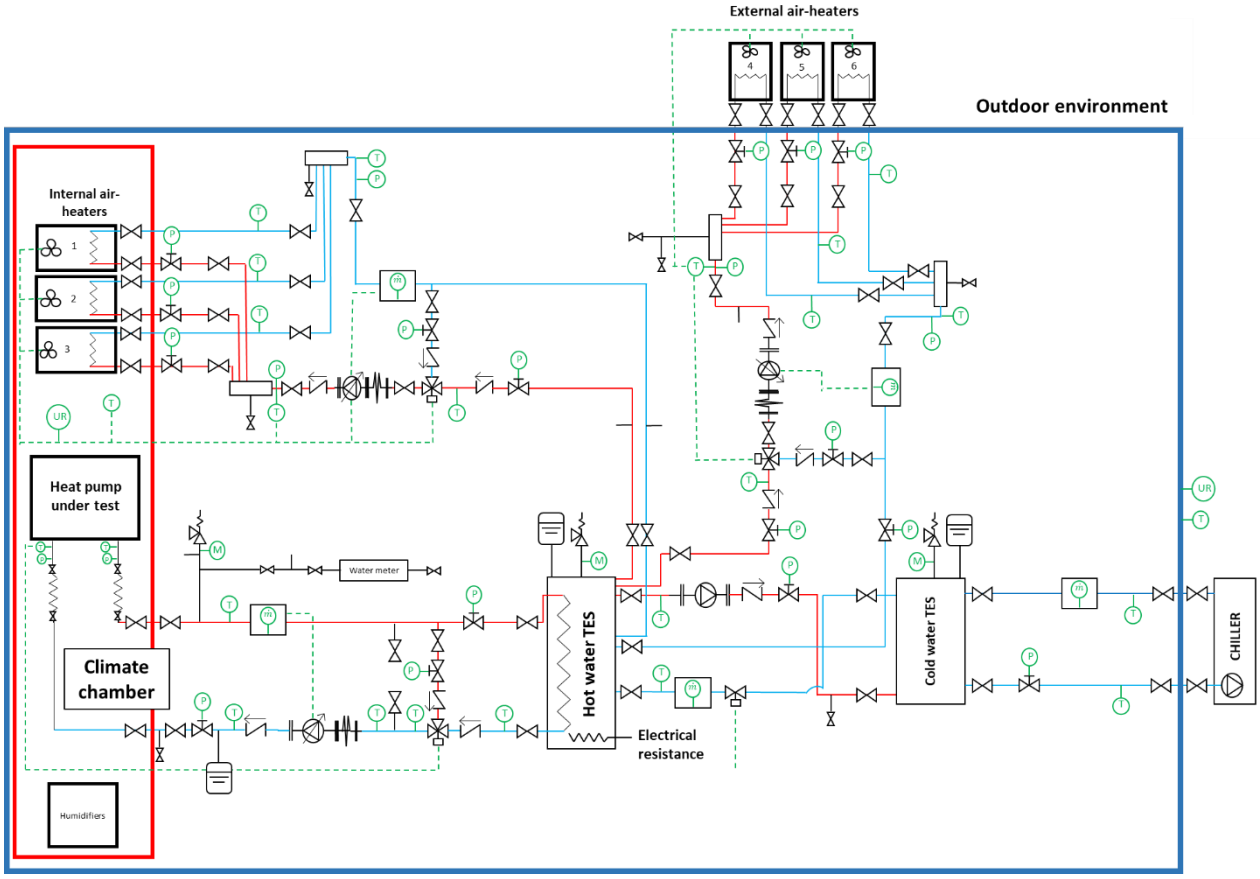

Figure 2. Hydraulic scheme of the experimental test rig (climate chamber within the red line).

In order to stabilize the system operation, a water thermal energy storage (TES) tank (hot water TES in Figure 2) is introduced in the hydronic loop. The tank has a volume of 0.5 m^3 (Figure 3b) and the hot water produced by the heat pump flows in a coiled heat exchanger, immersed within the tank, having a total external surface equal to 6 m^2 and a length of 60 m. The hot water TES is equipped with an electric resistance, having a heating capacity of 6 kW, used to provide additional energy when the heat delivered by the heat pump is not sufficient to maintain the CC temperature at the required value. The resistance also support the system during warm-ups and in particular operating conditions.

When CC air temperature has to be reduced, internal air-heaters fan speed decreases and, for this reason, the heat produced by the tested heat pump is discharged to the environment by means of three external air-heaters (components 4, 5 and 6 in Figure 2). Technical data of the six air-heaters installed in the test rig are reported in Table 2.

(a)

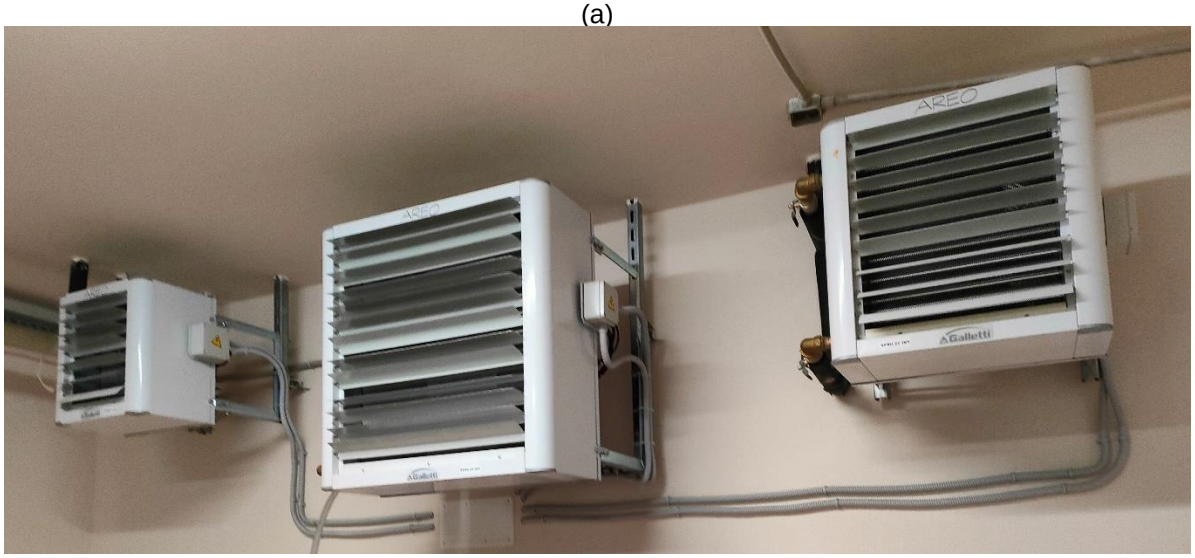

(b)

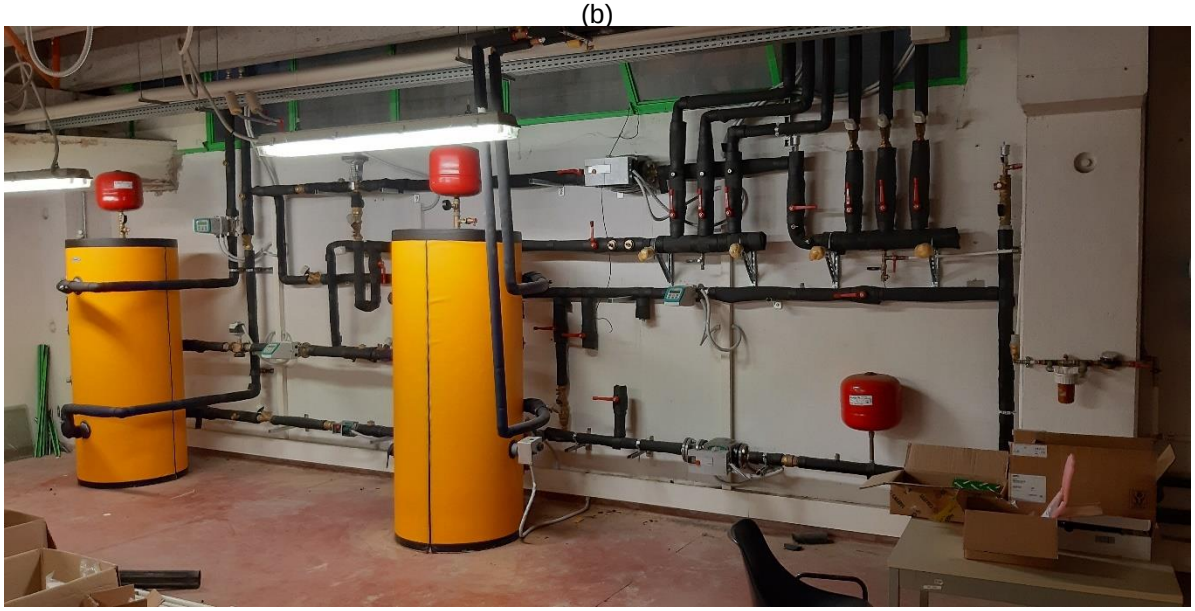

Figure 3. Air-heaters inside the climatic chamber (a) and the hydronic loop of the test rig (b).

When ambient air conditions do not guarantee the required heat transfer rate, an air-to-water inverter-driven chiller is operated. The conditioning unit is connected to a second thermal energy storage tank, having a volume of 0.5 m^3 (cold water TES in Figure 2). The cold water TES guarantees the stable operation of the system also when the chiller performs on-off cycles (i.e. when a low cooling power is needed). Table 3 reports the rated performance data of the chiller.

Temperature sensors and electromagnetic flow meters (Siemens, SITRANS F M MAG 1100, range 0-10 m/s, accuracy 0.2% ± 1 mm/s) are installed in the hydronic loop to check the operation of the whole system during experimental tests and to measure the

energy performance of the tested heat pump. A power meter has been also installed in the laboratory (Fluke 1735 three-phase power quality logger, accuracy ± 1 %) to analyze the electric power input of the heat pump under test.

T-type thermocouples and RTD Pt100 (accuracy class 1/10 DIN) calibrated in the range from -5°C to 50°C with an uncertainity of ± 0.15 K [34], are installed in the test bench.

When a GCHP or a DSHP (operating in ground mode) is tested, the heat pump heating capacity is dissipated thanks to the chiller or the external air-heaters. In this operation mode it is not necessary to control the CC conditions. In fact, when the heat pump operates in ground mode, the external heat source is the soil and heat is extracted through four vertical borehole heat exchangers (BHEs, see Figure 4). Different lengths of the vertical borefield can be considered: it is possible to combine, in different ways, two 100 m long and two 60 m long boreholes, obtaining undersized as well as oversized fields, to check the influence of BHE size on the heat pump performance.

Table 4 reports the technical data of the utilized measuring instruments: manufacturer, model, measuring range and uncertainty.

Table 2. Technical datasheet of internal and external air-heaters (Rated conditions: inlet air temperature = 15°C and inlet/outlet water temperature = 85-75°C).

Component	Modulation capability [%]	Rated heating capacity [W]	Maximum power absorbed [W]	Model	Location
Air-heater 1	20-100	11200	80	Galletti AREO12M0ECC0	Climate chamber
Air-heater 2	20-100	18700	139	Galletti AREO22M0ECC0	Climate chamber
Air-heater 3	20-100	67000	840	Galletti AREO43T0ECC0	Climate chamber
Air-heater 4	20-100	11200	80	Galletti AREO12M0ECC0	Outside the laboratory
Air-heater 5	20-100	18700	139	Galletti AREO22M0ECC0	Outside the laboratory
Air-heater 6	20-100	67000	840	Galletti AREO43T0ECC0	Outside the laboratory

Table 3. Technical data of the chiller (rated conditions: ambient air temperature = 35°C, inlet/outlet water temperature = 12/7°C).

Component	Frequency range [Hz]	Rated EER	Rated cooling capacity [W]	Maximum power [W]	Model	Location
Chiller	20-120	2.38	18200	22000	Galletti MPIDC018C0A	Outside the laboratory

Table 4. Technical data of the measuring instruments, including measuring range and uncertainty.

Model/sensor	Type	Range	Accuracy
Siemens SITRANS F M MAG 1100	Electromagnetic flow meter	0 – 10 m/s	0.2% ± 1 mm/s
Fluke 1735 three-phase power quality logger	Power meter	0 – 34.5 kW	± 1 %
RTD	Pt100 1/10 DIN	0 – 90 °C	± 0.03 K (at 0°C)
Thermocouples	T-type	0 – 90 °C	± 0.15 K

(a) (b)

Figure 4. Vertical borehole heat exchangers (a) and supply and return manifolds coupled to the boreholes field (b).

It is worth to mention that a Distributed Temperature Sensing (DTS) system is installed in the BHE field to measure the fluid thermal progression along different boreholes. More in detail, fiber optical cables are inserted inside two BHEs of different length (one 100 m and one 60 m long), Fiber optics are placed along the entire U-tube of the boreholes, measuring the fluid temperature distribution as a function of time when a heat pump is tested in ground-source mode and allowing to evaluate the depth-specific BHE thermal conductivity and thermal resistance [35].

The installed DTS system (SMARTEC, DiTemp Light Reading Unit) has a minimum spatial resolution of 2 m and a measurement time higher than 10 s. Temperature measurement accuracy depends on the calibration procedure, made with the same RTD Pt100 used for thermocouples calibration. DTS technology is based on Raman scattering, which occurs when the optical pulse energy is modified by changes in vibrational transition energy, caused by temperature variations. The ratio between stokes and anti-stokes Raman scattering is used to calculate the temperature, in conjunction with the time taken by the optical pulse to travel back to the DTS control unit.

3. Tests on ASHPs in steady-state conditions

In this Section, results of experimental tests carried out on an ASHP to determine its energy performance in steady-state condition, according to European standard UNI EN 14511-3 [36], are shown as a demonstrator of the potentiality of the test bench described in this work.

Several T-type thermocouples have been placed in the climate chamber to obtain accurate data on air temperature distribution. In Figures 5 and 6, the position of thermocouples is shown. The only readings used for the test evaluation according to standard [36] are sampled from thermocouples 1, 2, 4, 5, 8, 9 shown in Figures 5-6; those temperature sensors are placed in proximity of the evaporator of the heat pump under test. Data taken from the other thermocouples have no impact on the test outcomes but are useful to determine the temperature distribution in the chamber, as explained in the following sections.

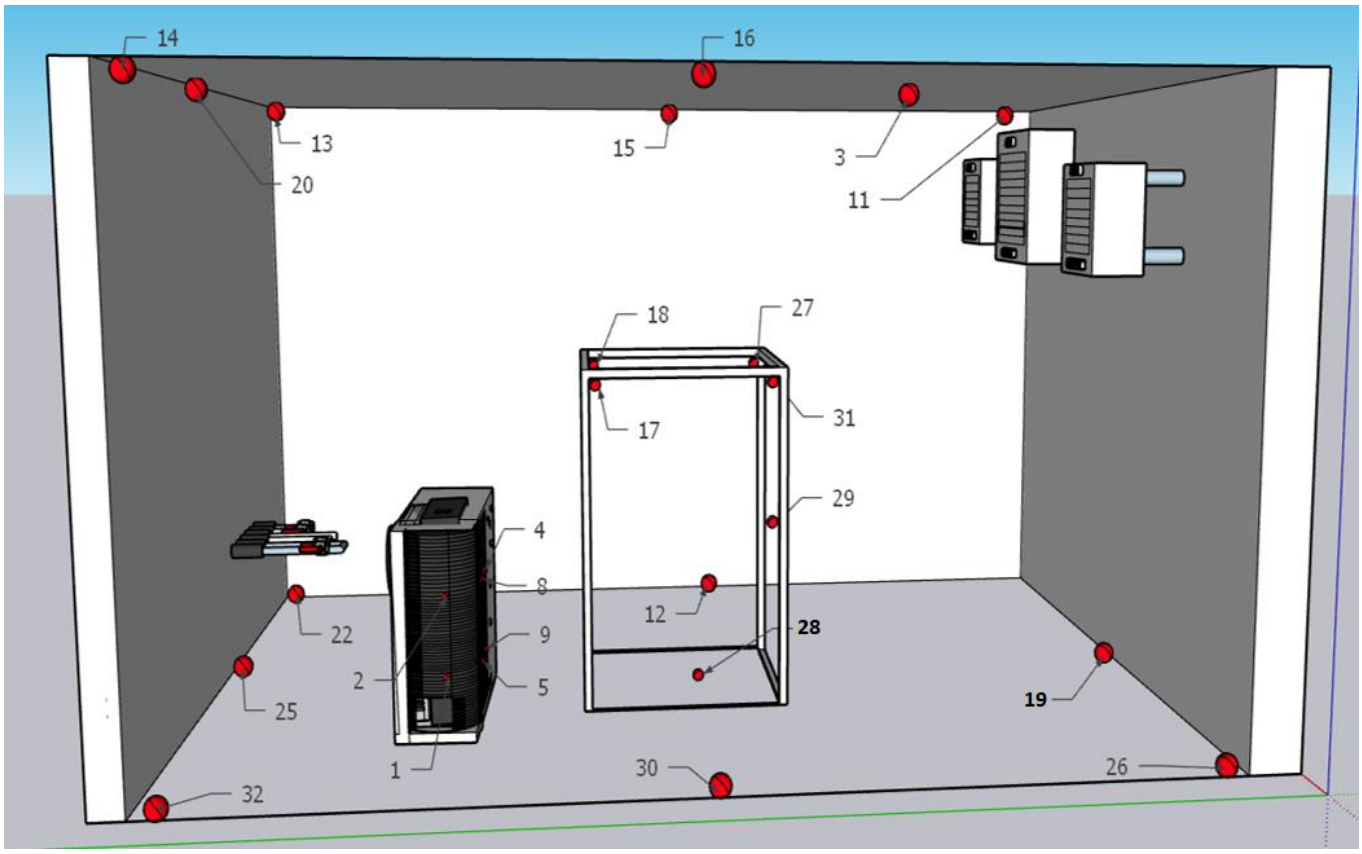

Figure 5. Position of the thermocouples (red dots) in the CC.

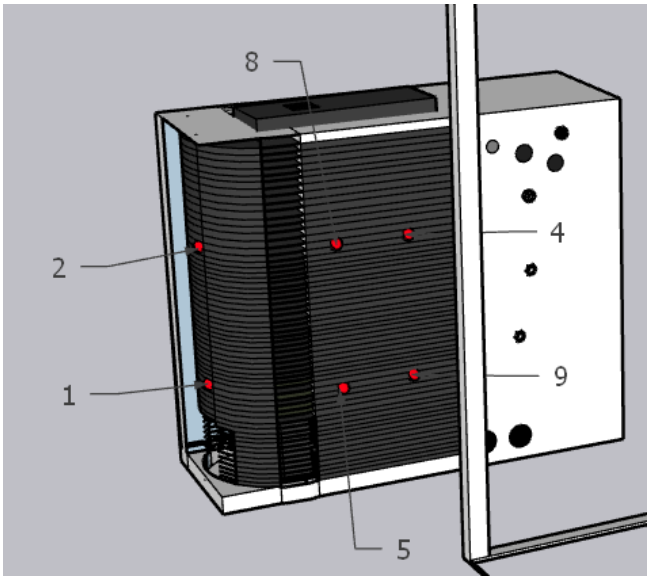

Figure 6. Position of the thermocouples (red dots) in proximity of the HP evaporator.

Figure 7. Heat pump inside the climate chamber (prototype based on mod. HWMC 010 HM).

The tested heat pump (Figure 7) is an air-source heat pump prototype, equipped with an inverter-driven compressor, and uses R-410A as refrigerant. The nominal thermal power is 11.4 kW, evaluated in the following conditions: air dry bulb and wet bulb temperature equal to 7°C and 6°C, respectively, water inlet and outlet temperature equal to 40°C and 45°C, respectively. In Figure 8, values of thermal power and *COP* given by the manufacturer are reported as functions of the external air temperature, for different inverter frequencies.

(a)

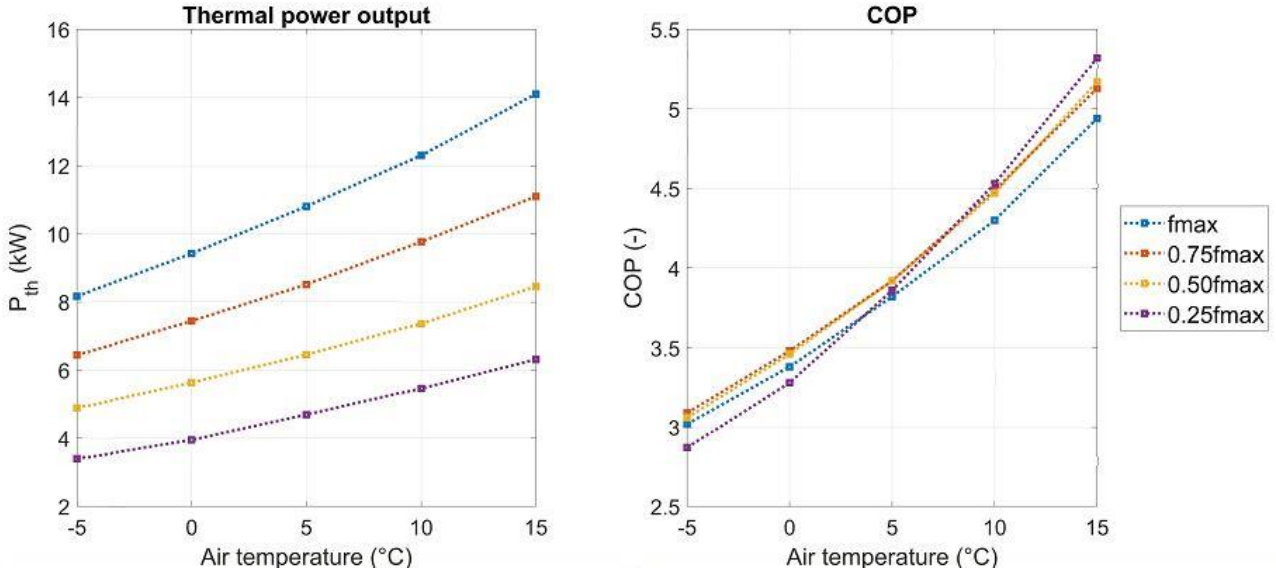

(b)

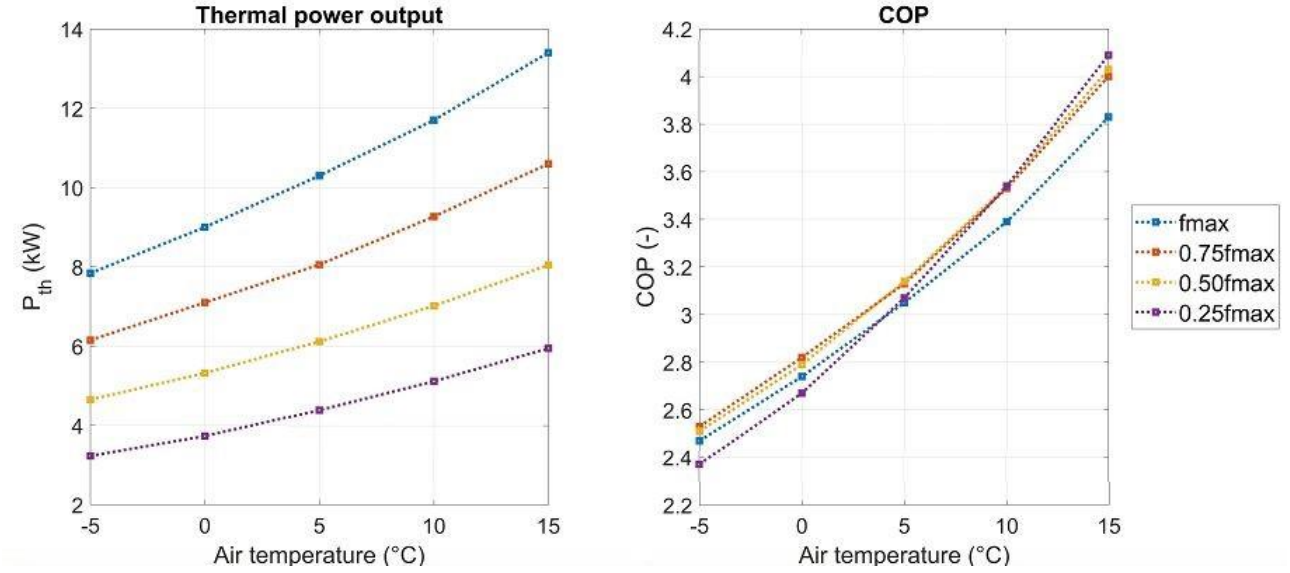

Figure 8. *COP* and thermal power output for the tested ASHP, referring to (a) inlet and outlet water temperature of 30 and 35°C, (b) inlet and outlet water temperature of 40 and 45°C.

Tests on the ASHP are carried out according to standard UNI EN 14511-3 procedure. The standard abovementioned prescribes to determine the heating capacity (P_{th}) of the air-to-water heat pump at the water side, measuring the water temperature difference (ΔT) and the water mass flow rate ($\dot{m}$) at the condenser of the heat pump under test, as follows:

$$P_{th} = \dot{m} c_p \Delta T \quad (1)$$

In Eq. (1), c_p is the specific heat capacity at constant pressure of the water flowing in the condenser, assumed constant during tests (4186 J/(kgK)).

Following the procedure reported in Eurovent technical standards for heat pump testing [37], sleeves for water temperature and pressure measurements at the heat pump inlet and outlet have been manufactured.

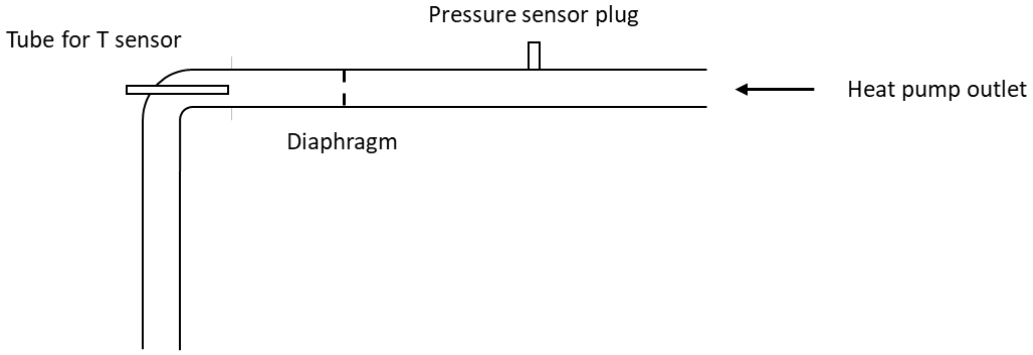

(a)

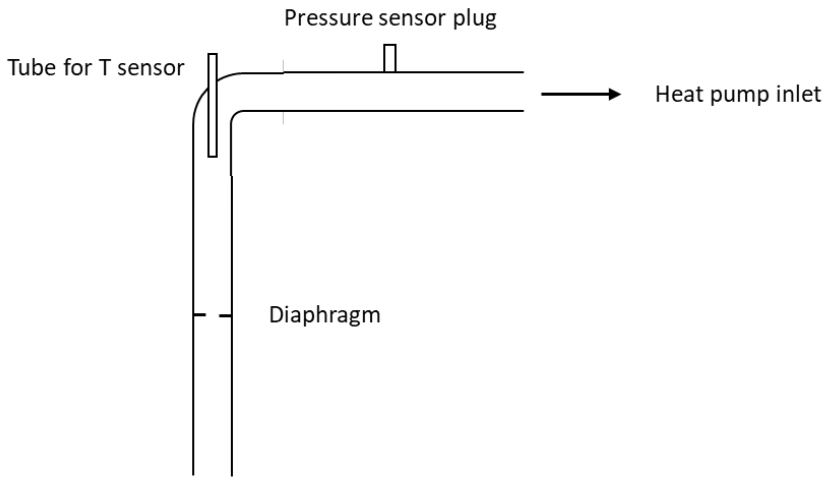

(b)

Figure 9. Sleeves for water temperature and pressure measurements at heat pump outlet (a) and inlet (b)

A scheme of the sleeves is reported in Figure 9. More in detail, each sleeve is composed by a plug for pressure measurements, located close to the heat pump, a diaphragm and a tube for the positioning of RTD temperature sensors. As pointed out by the figure, pressure plugs are installed close to the heat pump outlet/inlet ports in order to measure water pressure drops on the unit under test side. Furthermore, a diaphragm is inserted before each temperature sensor to introduce turbulence and, consequently to achieve uniform temperature measurements. According to the methodology reported by standard [37], temperature sensors are installed within an elbow, in a counterflow arrangement, and have a length of 100 mm. The distance between each diaphragm and the corresponding tube for temperature sensor housing is higher than 8 diameters. The standard also prescribes the test procedure, the specifications of the climate room and the admitted tolerances of the measuring equipment. An important aspect related to the climate chamber refers to the internal air flow distribution. The heat pump must be located away from the walls, with a minimum distance of 1 m, the air speed must be lower than 1.5 m/s and the air-heaters must not be placed close to the temperature sensors. The allowed measure uncertainties are specified in Table 5. At least 4 measuring points of the air temperature are necessary and sensors must be placed close to the evaporator of the heat pump under test (within 25 cm), evenly spaced.

Table 5. Maximum admitted uncertainty of measurement, prescribed by standard UNI EN 14511-3 [36].

Measured quantity	Maximum admitted uncertainty	Unit
Air dry bulb temperature	±0.2	K

Liquid inlet/outlet temperature	±0.15	K
Liquid temperature difference	±0.15	K
Liquid volume flow	±1%	
Electric power	±1%	

Tests in steady-state condition have been carried out for 70 minutes, collecting measurements every 30 s. In order to guarantee stationary conditions, test procedure reported by the standard [36] prescribes maximum fluctuations of temperature readings along the test. Table 6 shows the amplitude of allowed fluctuations. More in detail, two limits are reported by the standard: each single measurement should be included within a punctual range, while the average fluctuation along the test should be lower than the mean limit reported in Table 6.

Table 6. Maximum admitted measurement fluctuations during tests.

	Punctual	**Mean**
Inlet water temperature	±0.5 K	±0.2 K
Outlet water temperature	± 0.3 K	± 0.6 K
Air dry-bulb temperature	±1 K	±0.3 K

In addition, the standard prescribes to determine for every 5 minutes of the test the temperature difference between the water outlet and inlet of the heat pump. The mean temperature differences, measured every 5 minutes, are employed to determine the percentage temperature difference with respect to the mean temperature difference of the first 5 minutes of the test, using Eq.(2), where ΔT_0 refers to the mean value of the first five minutes and $\Delta T_i(\tau)$ refers to the mean temperature difference of the following 5 minutes intervals of the entire test,

$$\Delta T_{i,\%} = 100 \frac{\Delta T_0 - \Delta T_i(\tau)}{\Delta T_0}. \quad (2)$$

Standard EN 14511-3 prescribes that all the percentage temperature differences $\Delta T_{i,\%}$ must be less than 2.5%.

Table 7. Test conditions of the ASHP.

	Test 1	**Test 2**
Inlet water temperature	30 °C	40 °C
Outlet water temperature	35 °C	45 °C
Air dry-bulb temperature	7 °C	12 °C

Two tests have been carried out on the ASHP, to determine heat pump performance (i.e., heating capacity and *COP*) at full load. Operating conditions of both tests are reported in Table 7. In Table 8 minimum, maximum and mean temperature values of both air and water side during performed tests are reported.

Table 8. Mimimum, maximum and mean temperature values during tests.

	Test 1			Test 2		
Thermocouple	**Min (°C)**	**Max (°C)**	**Mean (°C)**	**Min (°C)**	**Max (°C)**	**Mean (°C)**
TC 1 (air - evaporator)	5.9	7.0	6.4	10.9	12.0	11.3
TC 2 (air - evaporator)	5.9	7.3	6.6	10.8	12.5	11.5
TC 4 (air - evaporator)	6.5	7.6	7.0	11.3	12.7	11.9
TC 5 (air - evaporator)	6.1	7.0	6.4	11.2	12.7	11.8
TC 8 (air - evaporator)	6.3	7.8	7.0	11.5	12.4	12.0
TC 9 (air - evaporator)	6.2	7.6	6.9	11.5	12.6	12.0
RTD 6 (HP water inlet)	29.9	30.2	30.0	40.0	40.2	40.1
RTD 7 (HP water outlet)	34.7	35.1	34.9	44.9	45.2	45.1

Results reported in Table 8 point out that for Test 1, TC 1 and TC 2 do not respect the prescribed tolerances, both for a single measure during the test and for the mean value. Moreover, also the average temperature value given by TC 5 does not respect the tolerance prescribed. On the contrary, if results of Test 2 are considered, punctual and mean limits are not satisfied by measures of TC 1 and TC 2. This aspect can be attributed to the non-uniform distribution of air temperature in the climate chamber and will be better investigated in the next section by means of CFD simulations.

In Table 9, values of absolute and relative water temperature difference between outlet and inlet of the heat pump are reported. Results show that the relative temperature difference was always less than 2.5% for the two tests carried out, as prescribed by the standard.

Finally, the energy performance of the tested ASHP are reported in Table 9, by considering the uncertainty propagation theory. In this table, the values of heating capacity and *COP* given by the heat pump manufacturer are reported as well.

Table 9. Water temperature difference between the ASHP inlet and outlet during tests.

	Test 1		Test 2	
Time (min)	ΔT_i (K)	$\Delta T_{i,\%}$ (%)	ΔT_i (K)	$\Delta T_{i,\%}$ (%)
5	4.90	-	4.99	-
10	4.88	0.47	5.00	-0.13
15	4.88	0.48	5.00	-0.12
20	4.86	0.74	5.00	-0.31
25	4.87	0.66	5.00	-0.22
30	4.89	0.18	4.99	0.05
35	4.88	0.46	4.99	0.03
40	4.89	0.16	4.99	-0.11
45	4.89	0.22	4.98	0.16
50	4.89	0.28	4.99	0.03
55	4.89	0.22	5.01	-0.35
60	4.89	0.24	5.00	-0.15
65	4.90	-0.06	4.98	0.12
70	4.89	0.12	5.00	-0.29

Table 10. Results from Test 1 and Test 2 compared to manufacturer data.

	Test 1 (experimental data)	Test 2 (experimental data)	Test 1 (declared by manufacturer)	Test 2 (declared by manufacturer)
Heating capacity (W)	10750±1370	11655±1450	11300	12300
COP (-)	3.48±0.52	3.16±0.46	3.98	3.55

Data in Table 10 show that the heat pump energy performance calculated experimenttally is lower than that declared by the manufacturer. Nevertheless, these values are in the range of the test results, if typical uncertainties values are considered. However we should note that, usually, manufacturers avoid to provide the accuracy range of the main nominal parameters indicated in their datasheet.

4. CFD analysis of air velocity and temperature field in the climate chamber

In this section, the results of CFD simulations, carried out by means of the software STAR-CCM+, are presented to study the air flow dynamics and the temperature distribution in the climate chamber during the test described before. The computational domain is shown in Figure 10, where the climate chamber is shown from two opposite views. The right hand side of the figure shows the ground, two vertical walls and the devices used for the air conditioning, i.e. the heat pump on the right and three air-heaters on the left. The left hand side of the figure shows the opposite view of the same room. The boundary conditions are the followings: a volume flow inlet from the air-heater equal to 1626 m^3/h (shown in red in the figure) and a volume flow rate from the heat pump equal to 7104 m^3/h (shown in blue). Moreover, outlet boundary conditions at the blue section in the air-heater and at the yellow section in the heat pump. The thermal power given to the inlet flow at the air-heater is 6.9 kW while the thermal power absorbed by the evaporator from the CC air is 8.35 kW. The transmittance of the walls has been set to 0.1 W/m^2 K, with an external temperature set to 30 °C.

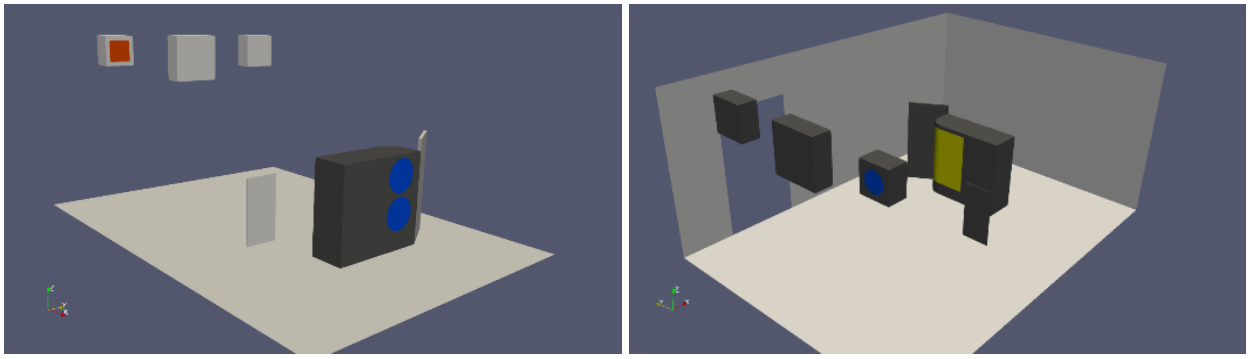

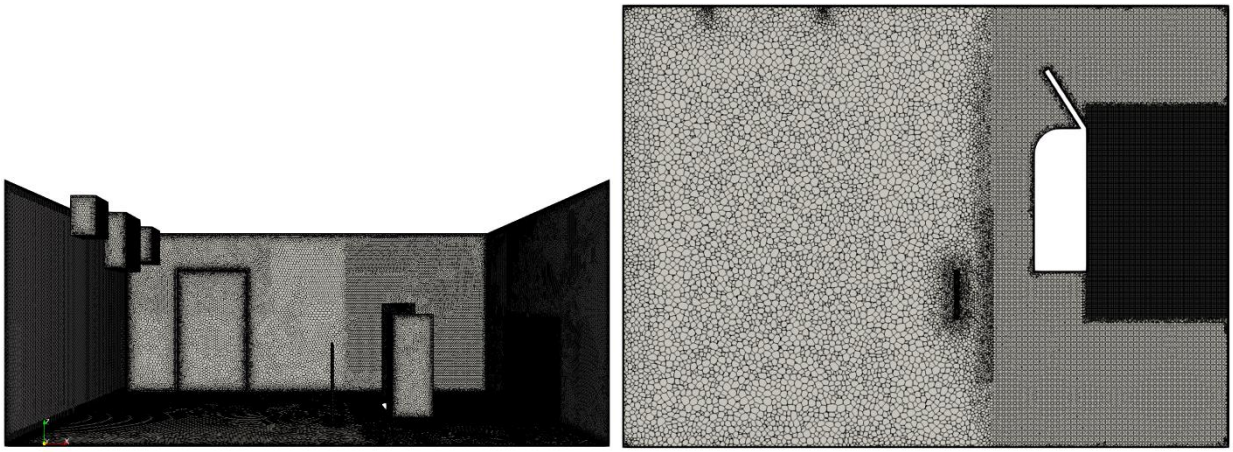

Figure 10. Two opposite views of the computational domain (top) and the mesh (bottom). Mesh of the elements and on the walls (bottom left) and on a horizontal section at 1 m (bottom right) .

Climate chamber envelope components are treated as walls with U-values obtained combining data shown in Table 1: the transmittance of floor and vertical walls is defined equal to 2 W/m^{2}K and 0.1 W/m^{2}K, respectively. The numerical simulations refer to the CC in a steady-state condition with a set-point temperature of 12°C. An unstructured mesh with polyedral elements has been built, as shown in Fig. 10.

The figure shows that three refinment zones have been considered, starting from the heat pump. A similar refinment zone have been built around the air-heater. A mesh convergency analysis has been made, starting from a mesh with 5 millions of elements up to a mesh with 25 millions of elements. The converged computational mesh has 20 million of elements. The Reynolds stress model has been used for modelling the turbulence, as it represents the most complete classical turbulence model. By this model, the eddy viscosity approach is avoided and the individual components of the Reynolds stress tensor are directly computed, to account for complex interactions in turbulent flow fields, such as the directional effects of the Reynolds stresses.

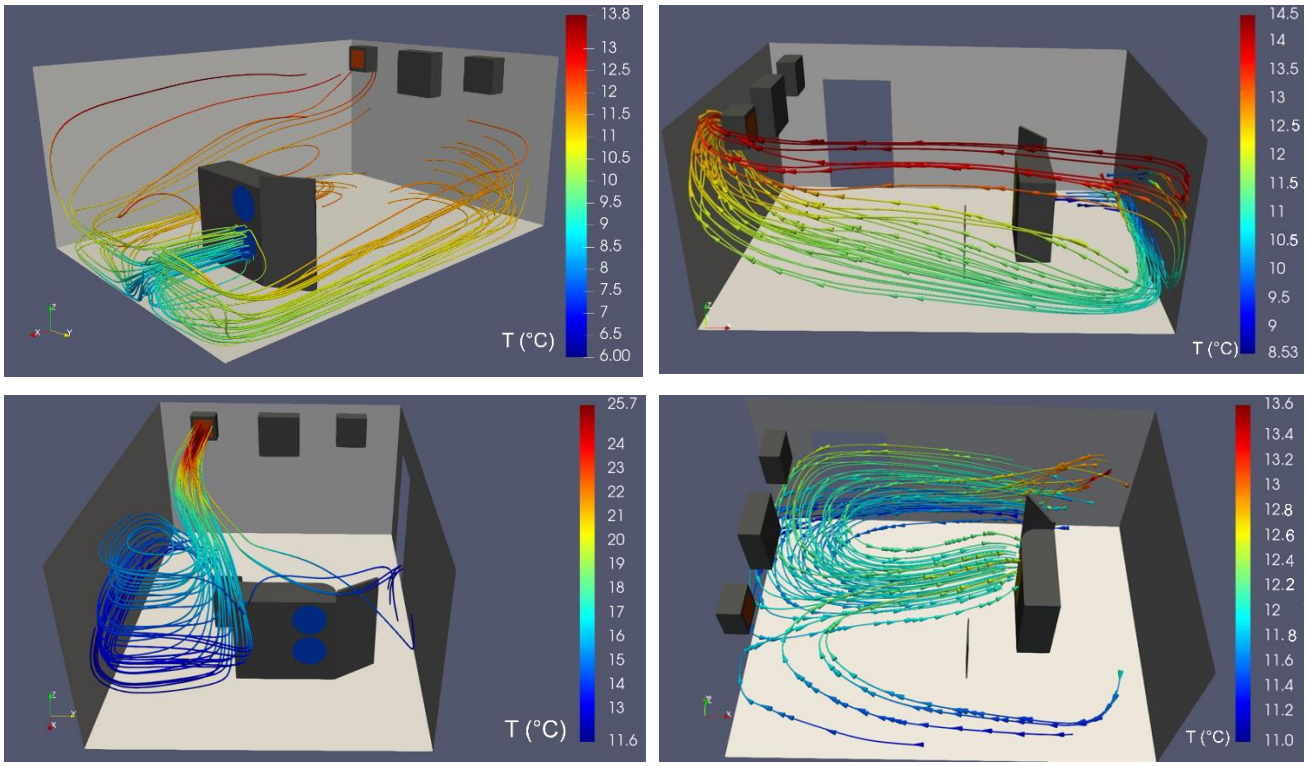

Figure 11. Streamlines obtained at the heat pump outlet (top, left), at the air-heater inlet (top, right), at the air-heater outlet (bottom, left) and at the heat pump inlet (bottom, right). The streamlines are coloured with the air temperature in Celsius degrees.

The streamlines coloured by the temperature obtained at the heat pump outlet are shown in Figure 11 top, left. The figure shows that the inlet cold air stream coming from the heat pump flows towards the wall, then, it is divided in two parts. The mainstream flows along the wall opposite to the side where the heaters are placed. The secondary stream flows along the opposite flow and is collected by the air-heater, as shown in Figure 11, top, right. Part of this stream is mixed with the flow coming from the air-heater in a vortex near the heat pump, as shown in Figure 11, bottom, left. The mainstream is then collected almost entirely by the heat pump, as shown by Figure 11, bottom, right. Figure 12 shows the velocity magnitude distribution and the vectors obtained on a horizontal plane at z=1 m. The velocity is less than 1.5 m/s, as requested by the standard UNI EN 14511-3. This plane is important because it is at a height where the devices which are tested within the climatic chamber are placed.

Figure 13 shows the air temperature distribution within the CC, obtained on horizontal planes at heights z=1 m and z=1.5 m. The temperature distribution obtained in the region between the heat pump and the wall where the heaters are placed is uniform with a value of 12 °C.

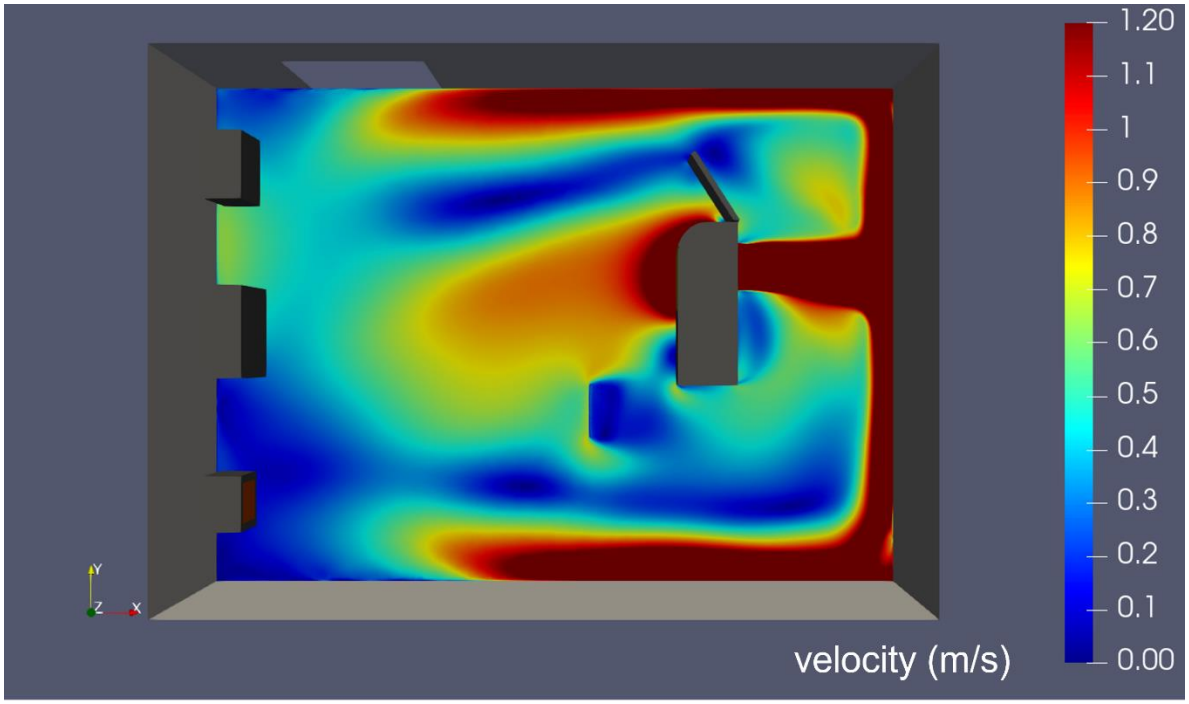
1.20
1.1
1
0.9
0.8
0.7
0.6
0.5
0.4
0.3
0.2
0.1
0.00
velocity (m/s)

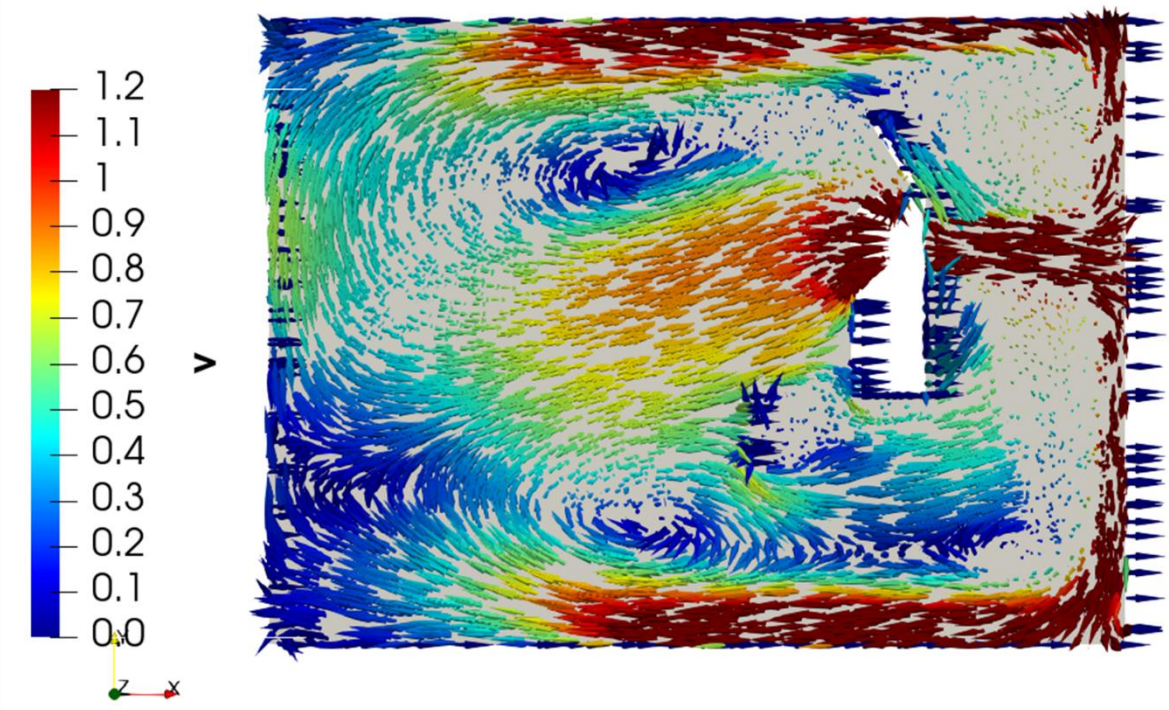
1.2
1.1
1
0.9
0.8
0.7
0.6
0.5
0.4
0.3
0.2
0.1
0.0
V

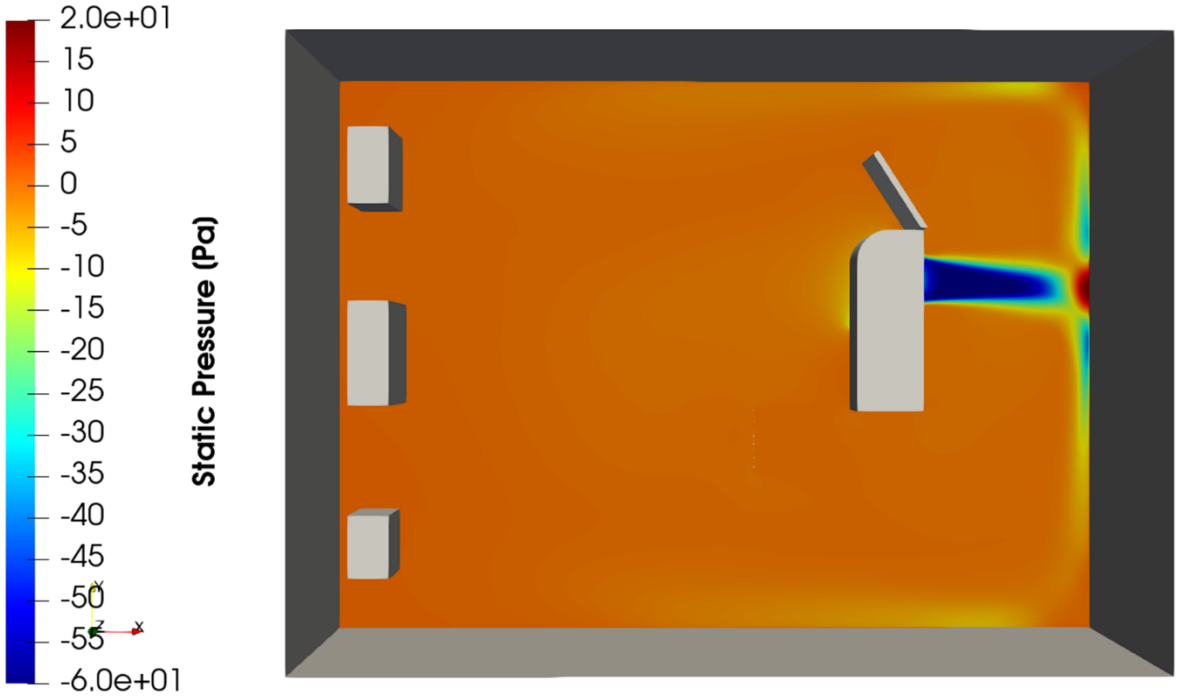

Figure 12. Velocity magnitude obtained on a horizontal plane at z=1.5 m (top), vectors on the same plane (middle) and static pressure distribution (bottom).

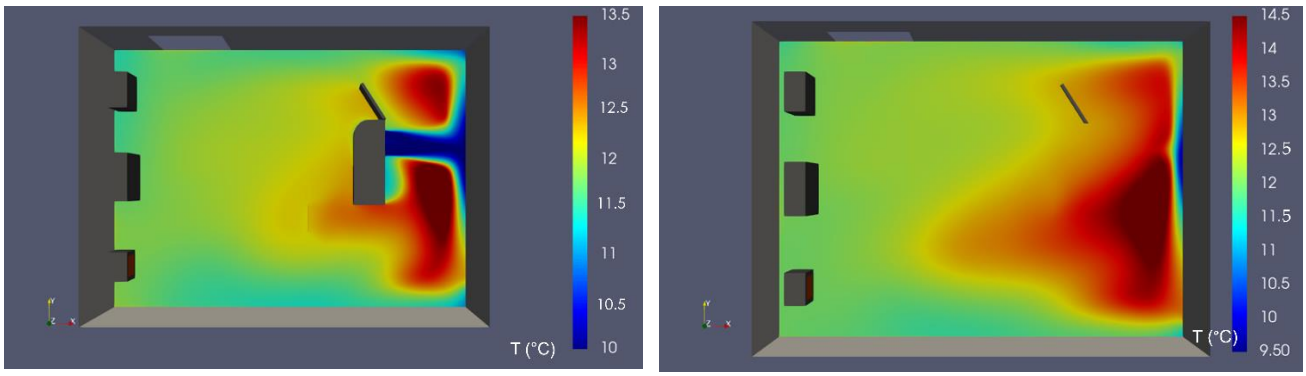

Figure 13. Temperature obtained on horizontal planes at z=1 m (left) and z=1.5 m (right).

Figures 11 and 12 show that there is a portion of the chamber near the heat pump where a strong peak of the velocity field is found. On the other side, the velocity and temperature fields are uniform. The vector map shown in Fig. 12 shows a zone with uniform velocity between two vortices. Near the wall this uniform velocity field shows velocities smaller than 0.5 m/s, with a uniform temperature distribution, as shown by fig. 13. In this region, also the static pressure is uniform, and this confirms the fact that the indicated area can be used for positioning the equipment to be tested in the climatic chamber. According to this outcome, it can be concluded that the optimal position of the heat pump under test has

been identified. This methodology can be helpful to assess the optimal installation of other heat pumps tested in the facility and, moreover, can predict whether the heat pump performs better in different positions with respect to that used in the tests described in this work. Furthermore, simulations show that the configuration implemented within the climate chamber (i.e., internal air-heaters placed on a side wall and tested heat pump on the opposite side of the chamber) can guarantee a controlled air temperature distribution within a zone in the room between the heater and the heat pump. Three positions have been chosen as representative of the average temperature of the chamber. These positions are shown in Figure 14 and the correspondent temperatures and velocities are shown in Table 11. These values have been compared with the measurements in order to validate the CFD simulations.

4.1 Comparison between CFD simulation and measured air temperature values in the CC

If we consider an enlarged view of Figure 13, considering the air temperature distribution at z=1 m from the floor and in proximity of the evaporator inlet (Figure 14), it can be noticed an uniform temperature of about 12°C, that is approximatively the same that was obtained by experimental data acquisition for the three thermocouples located at the heat pump evaporator inlet during the whole test 2 (TC 2, TC 4 and TC 8), as reported in Table 10.

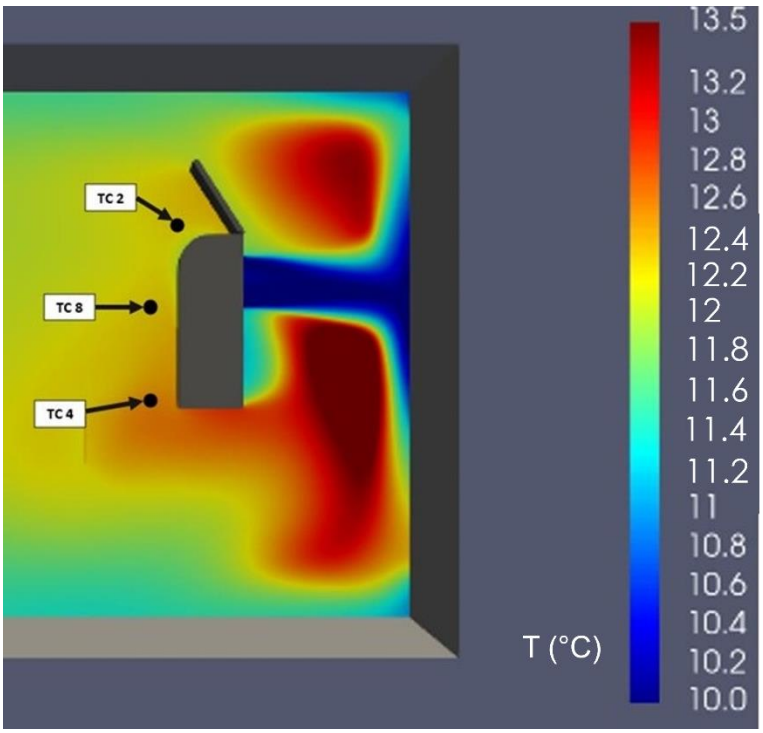

Figure 14. Temperature distribution in proximity of the evaporator inlet, at z=1 m from the floor.

Table 11. Mean air temperature values in proximity of the evaporator (mean value for the whole duration of test 2), temperature and velocity data obtained by CFD simulation.

Thermocouple	Velocity (m/s) CFD simulation	Temperature (°C) CFD simulation	Temperature (°C), test 2
TC 2	0.7	11.95	11.48
TC 4	0.8	12.09	11.88
TC 8	0.5	12.37	11.97

It can be observed that the measured temperature values are in good agreement with those obtained by CFD simulations. It can be concluded that these thermocouples provide an accurate indication of the average air temperature at the heat pump inlet and, for this reason, hose sensors can be taken as a reference to identify the setpoint temperature for the climatic chamber control. The measurements from the other thermocouples can be integrated to optimize the air flows in the chamber.

4.2. Dynamic simulations of the air temperature trend within the climate chamber

In order to investigate the trend of the air temperature in the climate chamber during a test, a numerical model of the climate chamber has been set up with Trnsys. In this model the climate chamber is considered as a single node characterized by a single value of internal air temperature which indicates the mean value of the air temperature in the room. Results given by the model are compared with experimental temperature measurements in the climate chamber with the aim to check if the thermal model of the climatic chamber made in TRNSYS is able to reproduce the observed experimental temperature trend within the chamber. The Trnsys model layout is reported in Figure 15.

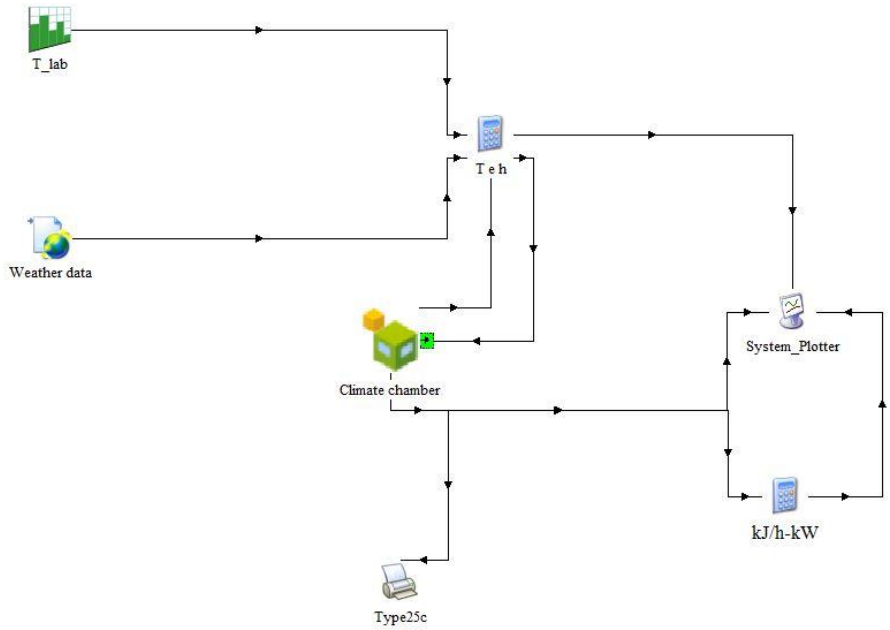

Figure 15. Layout of the Trnsys model for the analysis of climate chamber behavior.

The climate chamber envelope components are modelled by means of Trnsys Multizone building (type 56) by using the data reported in Table 1. The air change rate within the chamber is unknown and one of the indirect goals of this comparison is to use the experimental data to set the real value of the air change rate.

Dynamic simulations and experimental measurements aim to analyze the temperature variation in the CC when the mean air temperature value in the room (measured by 8 thermocouples, TC 17, TC 18, TC 22, TC 25, TC 27, TC 28, TC 30 and TC 32) reaches a steady-state value of 4°C and both air heaters and heat pump are switched off with an ambient temperature of 26.5°C. The time-step between measurements is set to 300 s. The dynamic simulations have been carried out assuming a time-step of 300 s, for a total of 60 h (the same of the experimental data acquisition). The air temperature inside the CC and the temperature of the air given by TRNSYS model are reported in Figure 16 as a function of time. We can observe a good agreement with experimental temperature measurements and simulated air temperature values if an air change rate of 0.5 h^{-1} is imposed. The mean percentage relative difference between experimental and numerical data is about 2%. After 60 h the mean temperature within the chamber reaches 21°C, 6.6 K less than the ambient temperature. During the first 13 hours after the switch-off, temperature tends to increase with an average rate of 1.06 K/h. This value is important for the correct setup of

556 the CC control system. These results confirm the good thermal insulation level of the
557 climate chamber.
558

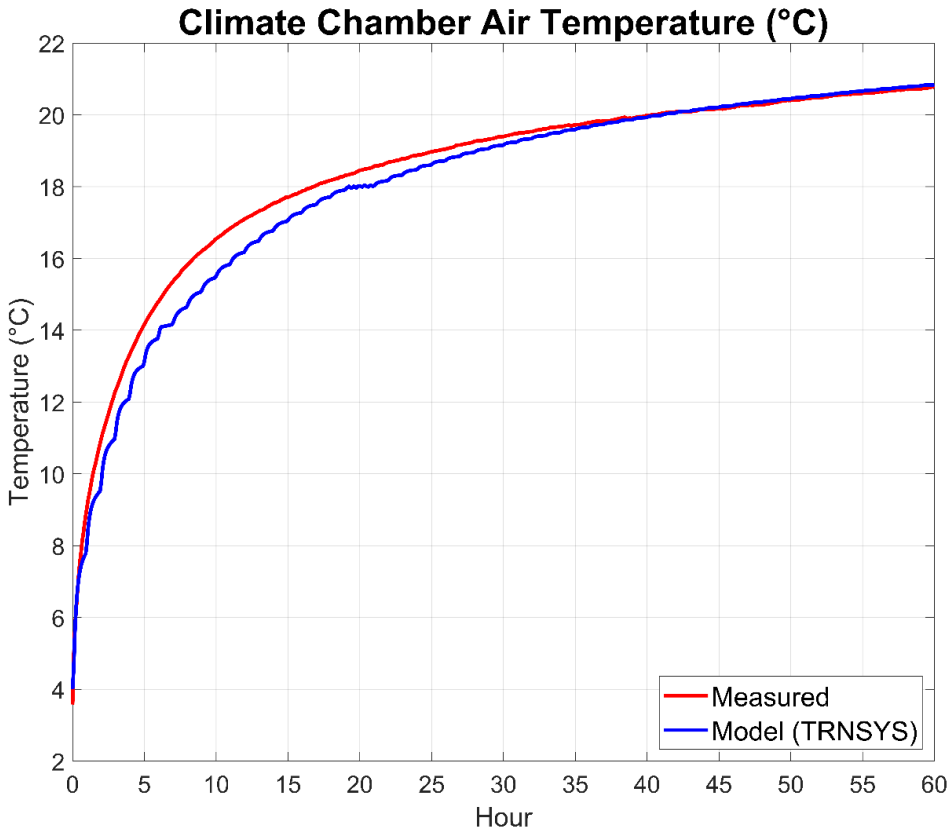

559
560 Figure 16. Comparison between measured and simulated dlimate chamber air
561 temperature.
562
563 **5. Conclusions**
564 In this paper, the layout and the working principle of a new experimental test rig, designed
565 and realized at the University of Bologna,Italy, are described. The main purpose of the set-
566 up is to test air-source and ground-coupled heat pumps, having a rated heating capacity
567 lower than 12 kW, through the Hardware-in-the-Loop approach. Main elements of the test
568 rig are: a highly-insulated climate chamber, in which the tested heat pump is placed; the
569 hydraulic circuit used to manage the system; the building emulator, by means of which the
570 thermal load of a building is calculated through dynamic simulations and given to the loop;
571 a borehole heat exchanger field for tests on ground-source heat pumps.
572 In this paper, the importance of numerical simulation software, such as Trnsys, Matlab-
573 Simulink and STAR-CCM+, in the design of the climate chamber has been also
574 demonstrated. It has been shown that numerical simulations are important during the

575 design phase of this kind of test rigs and, moreover, dynamic simulations are pivotal also
576 for the setup of the Hardware-in-the Loop control system. Then, some experimental
577 measures on a commercial air-source heat pump, carried out according to current
578 standard UNI EN 14511-3, are described as trial test for the facility. Numerical models
579 have been then validated with experimental data. The comparison between experimental
580 results and data reported in the manufacturer datasheet confirms a good agreement,
581 pointing out the reliability of the test rig described in this work. With the help of CFD, air
582 velocity and temperature distribution within the room have been obtained as a function of
583 the position of the heat pump in the chamber and of the activated air-heaters. Outcomes of
584 this work demonstrate how a cross-validation methodology combining numerical and
585 experimental data is crucial during the design phase of test facilities as the one presented
586 in this paper. In fact, according to that methodology, the uniformity of temperature
587 distribution within the chamber and the air velocity field close to the heat pump can be
588 verified in order to assess the optimal position of the heat pump within the room. Finally, it
589 is expected that the HiL system described in this paper will become an important design
590 tool for heat pump manufacturers to evaluate experimentally the effective performance of
591 heat pump-based HVAC systems.
592
593 **Acknowledgements**
594 The research leading to these results has received funding from MUR within the
595 framework of the PRIN2017 project «The energy FLEXibility of enhanced HEAT pumps for
596 the next generation of sustainable buildings (FLEXHEAT)», grant 2017KAAECT.
597
598 **Nomenclature**

599 A, B, C, D	walls of the climate chamber
600 ASHP	air-source heat pump
601 BE	building emulator
602 BHE	borehole heat exchanger
603 CC	climate chamber
604 *COP*	coefficient of performance of a heat pump
605 c_p	specific heat capacity at constant pressure [J/(kg K)]
606 DSHP	dual source heat pump
607 DTS	Distributed Temperature Sensing system
608 GSHP	ground-source heat pump

HiL	hardware-in-the-loop
$\dot{m}$	mass flow rate [kg/s]
P_{th}	heating capacity of an air-to-water heat pump [W]
Q	thermal power [W]
TC	thermocouple
Z	vertical coordinate [m]
ΔT	water temperature difference [K]
ΔT_0	mean water temperature difference of the first five minutes of test
$\Delta T_i(\tau)$	mean water temperature difference of the following 5 minutes intervals of the entire test

References

[1] European Parliament and Council. REPowerEU Plan. Communication from the Commission to the European Parliament, the European Council, the European Economic and Social Committee and the Committee of the Regions, https://eur-lex.europa.eu/legal-content/EN/TXT/?uri=COM%3A2022%3A230%3AFIN&qid=1653033742483 (Accessed August 29th 2022)

[2] European Parliament and Council. 2018. Directive (EU) 2018/2001 of the European Parliament and of the Council of 11 December 2018 on the promotion of the use of energy from renewable sources. Official Journal of the European Union.

[3] I. Sarbu, C. Sebarchievici, General review of ground-source heat pump systems for heating and cooling of buildings, Energy Build 70 (2014),441–454.

[4] P. Carroll, M. Chesser, P.Lyons P, Air Source Heat Pumps field studies: A systematic literature review, Renew Sust Energ Rev 134 (2020), 1-12.

[5] European heat pump association (EHPA). European heat pump market and statistics report, 2021, https://www.ehpa.org/market-data/market-report-2021/ (Accessed August 29th 2022).

[6] M. Dongellini, C. Naldi, G.L. Morini, Influence of sizing strategy and control rules on the energy saving potential of heat pump hybrid systems in a residential building, Energy Convers Manag 235 (2021):114022.

[7] G. Bagarella, R. Lazzarin, M. Noro, Sizing strategy of on-off and modulation heat pump systems based on annual energy analysis, Int J Refrig 65 (2016),183-193.

[8] Y. Zhang, G., Zhang, A. Zhang, Y. Jin, R.Ru, M. Tian, Frosting phenomenon and frost-free technology of outdoor air heat exchanger for an air-source heat pump system in China: An analysis and review, Energies 11 (2018), 1-36.

[9] E. R, Di Schio, V. Ballerini, M. Dongellini, P. Valdiserri, Defrosting of air-source heat pumps: Effect of real temperature data on seasonal energy performance for different locations in italy, Appl Sci 11 (2021) 8003.

[10] Z. Xi, R. Yao, J. Li, C. Du, Z. Yu, B. Li, Experimental studies on hot gas bypass defrosting control strategies for air source heat pumps, J. Build. Eng. *43* (2021) 103165.

[11] P. Vocale, G.L. Morini, M. Spiga, Influence of outdoor air conditions on the air source heat pumps performance, Energy Procedia 45 (2014), 653-662.

[12] M. Lucchi, M. Lorenzini, P. Valdiserri, Energy performance of a ventilation system for a block of apartments with a ground source heat pump as generation system, J Phys Conf Ser 796 (2017), 1-9.

[13] T. You, W. Wu, W. Shi, W. Baolong, X. Li, An overview of the problems and solutions of soil thermal imbalance of ground coumpled heat pumps in cold regions, Appl Energy 177 (2016) 515-536.

[14] A. Jahanbin, G. Semprini, A.N. Impiombato, C. Biserni, E.R. Di Schio , Effects of the circuit arrangement on the thermal performance of double U-tube ground heat exchangers, Energies 13 (2020) 3275.

[15] A.A. Safa, A.S. Fung, R. Kumar, Comparative thermal performances of a ground source heat pump and a variable capacity air source heat pump systems for sustainable houses, Appl Therm Eng 81 (2015) 279-287.

[16] S.J. Self, B.V. Reddy, M.A. Rosen, Geothermal heat pump systems: Status review and comparison with other heating options, Appl Energy 101 (2013) 341-348.

[17] X. L., L. Fu, S.G. Zhang, Y. Jiang, Z.L. Lai, Study of the performance of an urban original source heat pump system, Energy Convers Manag 4 (2010) 765-770.

[18] S. Ran, W. Lyu, X. Li, W. Xu, B. Wang, A solar-air source heat pump with thermosiphon to efficiently utilize solar energy, J. Build. Eng. 31 (2020), 101330.

[19] G. Quirosa, M. Torres, V.M. Soltero, R. Chacartegui, Energetic and economic analysis of decoupled strategy for heating and cooling production with CO_2 booster heat pumps for ultra-low temperature district network, J. Build. Eng. 45(2022), 103538.

[20] R.M. Lazzarin, Dual source heat pump systems: Operation and performance. Energy Build 52 (2012) 77-85.

675 [21] I. Grossi, M. Dongellini, A. Piazzi, G.L. Morini, Dynamic modelling and energy
676 performance analysis of an innovative dual-source heat pump system, Appl Therm Eng
677 142 (2018) 745-759.
678 [22] S.A. Klein, W.A. Beckman, J.W. Mitchell, J.A. Duffie, N.A. Duffie, T.L. Freeman,
679 J.C. Mitchell, J.E. Braun, B.L. Evans, J.P. Kummer, et al., TRNSYS Version 18; Solar
680 Energy Laboratory, University of Wisconsin-Madison: Madison, WI, USA (2018).
681 [23] P. Valdiserri, E.R. Di Schio, V. Rondelli, E. Capacci, A numerical analysis for the
682 design of a climatic chamber, AIP Conference Proceedings 2191 (2019), 020150.
683 [24] P. Haves, A. Dexter, D.R. Jorgensen, K.V. Ling, G. Geng, Use of a building
684 emulator to develop techniques for impreved commissioning and control of HVAC system,
685 ASHRAE Transaction 97 (1991) 684-688.
686 [25] R. Lahrech, P. Gruber, P. Riederer, P. Tessier, J.C. Visier, Development of a testing
687 method for control HVAC systems by emulation, Energy Build 34 (2002) 909-916.
688 [26] M. Anderson, M. Buehner, P. Young, D. Hittle, C. Anderson, J. Tu, D. Hodgson, An
689 experimental system for advanced heating, ventilating and air conditioning (HVAC) control,
690 Energy Build 39 (2007) 136-147.
691 [27] A.T. De La Cruz, P. Riviere, D. Marchio, O. Cauret, A. Milu, Hardware in the loop
692 test bench using Modelica: A platform to test and improve the control of heating systems,
693 Appl Energy 188 (2017) 107-120.
694 [28] P. Conti, C. Bartoli, A. Franco, D. Testi, Experimental Analysis of an Air Heat Pump
695 for Heating Service Using a “Hardware-In-The-Loop” System, Energies 13 (2020) 1-18.
696 [29] L. Frison, M. Kleinstück, P. Engelmann, Model-predictive control for testing energy
697 flexible heat pump operation within a Hardware-in-the-Loop, J Phys Conf Ser 1343 (2019)
698 1-6.
699 [30] P. Mehrfeld, M. Nürenberg, M. Knorr, L. Schinke, M. Beyer, M. Grimm, M. Lauster;
700 D. Müller, J. Seifert, K. Stergiaropoulos, Dynamic evaluations of heat pump and micro
701 combined heat and power systems using the hardware-in-the-loop approach, J Build Eng
702 28 (2020) 1-14.
703 [31] Matlab-Simulink software, https://it.mathworks.com/products/simulink.html
704 (Accessed August 29th 2022).
705 [32] Solar-Institut Juelich, CARNOT-Blockset, 1999. Germany Scientific Computers
706 GmbH.

[33] J.P. Campana, G.L. Morini, BESTEST and EN ISO 52016 Benchmarking of ALMABuild, a New Open-Source Simulink Tool for Dynamic Energy Modelling of Buildings, Energies 12, (2019), 2938.

[34] R.J. Moffat, Describing the uncertainties in experimental results, Exp. Thermal Fluid Sc. 1 (1998) 1-17.

[35] J. Acuña, B. Palm, Distributed thermal response tests on pipe-in-pipe borehole heat exchangers, Appl. Energy 109 (2013) 312-320.

[36] UNI EN 14511-3:2018, Air conditioners, liquid chilling packages and heat pumps for space heating and cooling and process chillers, with electrically driven compressors - Part 3: Test methods.

[37] EUROVENT, Third party certification - Certita Eurovent, https://www.eurovent-certification.com/en (Accessed August 29th 2022).